

AFRL-ML-WP-TR-2006-4248

**COLLABORATIVE RESEARCH AND
DEVELOPMENT**

**Delivery Order 0006: Transmission Electron
Microscope Image Modeling and
Semiconductor Heterointerface
Characterization**

Krishnamurthy Mahalingam, Ph.D.

**Universal Technology Corporation
1270 North Fairfield Road
Dayton, OH 45432-2600**



SEPTEMBER 2006

Final Report for 19 May 2003 – 18 May 2006

Approved for public release; distribution is unlimited.

STINFO COPY

**MATERIALS AND MANUFACTURING DIRECTORATE
AIR FORCE RESEARCH LABORATORY
AIR FORCE MATERIEL COMMAND
WRIGHT-PATTERSON AIR FORCE BASE, OH 45433-7750**

NOTICE AND SIGNATURE PAGE

Using Government drawings, specifications, or other data included in this document for any purpose other than Government procurement does not in any way obligate the U.S. Government. The fact that the Government formulated or supplied the drawings, specifications, or other data does not license the holder or any other person or corporation; or convey any rights or permission to manufacture, use, or sell any patented invention that may relate to them.

This report was cleared for public release by the Air Force Research Laboratory Wright Site (AFRL/WS) Public Affairs Office and is available to the general public, including foreign nationals. Copies may be obtained from the Defense Technical Information Center (DTIC) (<http://www.dtic.mil>).

AFRL-ML-WP-TR-2006-4248 HAS BEEN REVIEWED AND IS APPROVED FOR PUBLICATION IN ACCORDANCE WITH ASSIGNED DISTRIBUTION STATEMENT.

*/Signature//

RITA SCHOLES
Project Manager
Business Operations Branch
Integration and Operations Division

//Signature//

ROBERT ENGHAUSER
Acting Chief
Business Operations Branch
Integration and Operations Division

This report is published in the interest of scientific and technical information exchange, and its publication does not constitute the Government's approval or disapproval of its ideas or findings.

*Disseminated copies will show “//signature//” stamped or typed above the signature blocks.

REPORT DOCUMENTATION PAGE

*Form Approved
OMB No. 0704-0188*

The public reporting burden for this collection of information is estimated to average 1 hour per response, including the time for reviewing instructions, searching existing data sources, searching existing data sources, gathering and maintaining the data needed, and completing and reviewing the collection of information. Send comments regarding this burden estimate or any other aspect of this collection of information, including suggestions for reducing this burden, to Department of Defense, Washington Headquarters Services, Directorate for Information Operations and Reports (0704-0188), 1215 Jefferson Davis Highway, Suite 1204, Arlington, VA 22202-4302. Respondents should be aware that notwithstanding any other provision of law, no person shall be subject to any penalty for failing to comply with a collection of information if it does not display a currently valid OMB control number. **PLEASE DO NOT RETURN YOUR FORM TO THE ABOVE ADDRESS.**

1. REPORT DATE (DD-MM-YY) September 2006			2. REPORT TYPE Final		3. DATES COVERED (From - To) 05/19/2003 – 05/18/2006	
4. TITLE AND SUBTITLE COLLABORATIVE RESEARCH AND DEVELOPMENT Delivery Order 0006: Transmission Electron Microscope Image Modeling and Semiconductor Heterointerface Characterization			5a. CONTRACT NUMBER F33615-03-D-5801-0006			
			5b. GRANT NUMBER			
			5c. PROGRAM ELEMENT NUMBER 62102F			
6. AUTHOR(S) Krishnamurthy Mahalingam, Ph.D.			5d. PROJECT NUMBER 4349			
			5e. TASK NUMBER L0			
			5f. WORK UNIT NUMBER VT			
7. PERFORMING ORGANIZATION NAME(S) AND ADDRESS(ES) Universal Technology Corporation 1270 North Fairfield Road Dayton, OH 45432-2600			8. PERFORMING ORGANIZATION REPORT NUMBER S-531-006			
9. SPONSORING/MONITORING AGENCY NAME(S) AND ADDRESS(ES) Materials and Manufacturing Directorate Air Force Research Laboratory Air Force Materiel Command Wright-Patterson AFB, OH 45433-7750			10. SPONSORING/MONITORING AGENCY ACRONYM(S) AFRL-ML-WP			
			11. SPONSORING/MONITORING AGENCY REPORT NUMBER(S) AFRL-ML-WP-TR-2006-4248			
12. DISTRIBUTION/AVAILABILITY STATEMENT Approved for public release; distribution is unlimited.						
13. SUPPLEMENTARY NOTES PAO Case Number: AFRL/WS 06-2820, 07 Dec 2006. Report contains color.						
14. ABSTRACT (Maximum 200 words) <p>This research in support of the Air Force Research Laboratory, Materials and Manufacturing Directorate was conducted at Wright-Patterson AFB, Ohio from 19 May 2003 through 18 May 2006. Transmission electron microscope (TEM) characterization studies were performed on a variety of novel III-V semiconductor heterostructures being developed for advanced optoelectronic device applications. A new approach is developed for true atomic scale compositional mapping of interfaces in mixed cation-anion III-V semiconductor heterostructures. This approach is applied for quantifying stoichiometry of interfaces in InAs/InGaSb superlattices. Detailed TEM studies were performed on short-period InAs/GaSb superlattices with periods ranging from 50Å to 11Å. Significant degradation in structural quality was observed with reduction in the superlattice period. Improvement in quality is however achieved by reducing the growth rate (specifically in the GaSb growth rate). The formation of heterojunction quantum dots (QD) composed of a combination of InAs and GaSb is demonstrated. The composite dot is achieved by first forming InAs QDs by normal self assembly process followed by growth of a GaSb crown atop the InAs QD structure. Transmission electron microscopy indicated a clear boundary between the GaSb and InAs regions with energy dispersive spectroscopy analysis showing an In rich core and a Sb rich cap.</p>						
15. SUBJECT TERMS						
16. SECURITY CLASSIFICATION OF: b. REPORT Unclassified			17. LIMITATION OF ABSTRACT: SAR	18. NUMBER OF PAGES 50	19a. NAME OF RESPONSIBLE PERSON (Monitor) Rita Scholes	
c. ABSTRACT Unclassified			19b. TELEPHONE NUMBER (Include Area Code) N/A			

TABLE OF CONTENTS

	Page
FIGURES	iv
SUMMARY	1
1.0 INTRODUCTION	3
2.0 EXPERIMENTAL PROCEDURE.....	4
3.0 RESULTS AND DISCUSSION.....	5
3.1 Quantifying Stoichiometry of III-V Semiconductor Interfaces.....	5
3.2 TEM of InAs/GaSb Short-Period Superlattices.....	23
3.3 TEM of Heterojunction Quantum Dot Structures	28
4.0 CONCLUSIONS.....	37
REFERENCES	38

LIST OF FIGURES

Figure	Page
3.1 (a) Reconstructed phase image of Al _{0.6} Ga _{0.4} As/GaAs interfaces, where the position of each interface is denoted by an arrow, (b) profile along Al-Ga sites, denoted by line a-b, and (c) profile along the As sites, denoted by line c-d	8
3.2 (a) Reconstructed phase image of In _{0.25} Ga _{0.75} Sb/InAs interfaces, where the position of each interface is denoted by an arrow, (b) profile along In-Ga sites, denoted by line a-b, and (c) profile along the As-Sb sites, denoted by line c-d.....	11
3.3 Flow chart describing the different steps employed in the factor analysis procedure.....	14
3.4 (a) A simulated EPWF-phase image of a Al _{0.4} Ga _{0.6} As/GaAs/Al _{0.4} Ga _{0.6} As model structure with an abrupt interface and a graded interface and (b) a plot of C ₁ for each unit cell across the interface calculated for specimen thickness of 6.7nm.....	15
3.5 A plot showing the variation of C ₁ for an InAs/ In _{0.25} Ga _{0.77} Sb model structure with an abrupt interface on one side and a linear grading in both the In/Ga and As/Sb sublattices on the other, for a specimen thickness of 6nm. The inset shows the eigenvector images for the In-Ga and the As-Sb sublattices onto which each unit cell was projected to obtain C ₁	17
3.6 (a) Composition map showing variation of C ₁ from the experimental EPWF-phase image for AlGaAs/GaAs interface shown in Fig. 1(a), and (b) profile of x _{Al} and C ₁ normal to the interface and averaged over unit cells parallel to the interface.....	20
3.7 (a) Composition maps of the phase image in Fig. 2(a), showing the variation of the FAC coefficient C ₁ within (a) the In-Ga sublattice and (b) the As-Sb sublattice. The arrows locate the interfacial regions in Fig. 2 (a), and (c) compositional profiles of the In-Ga and As-Sb sublattices showing the mean compositions, x _{Ga} and x _{Sb} , of each atomic layer along the [100] direction in Fig. 2(a)	22

3.8 (a) A (200) dark-field image and (b) a [010] cross-sectional HRTEM image of an InAs-GaSb superlattice structure showing smooth and abrupt interfaces between the individual layers. The intended individual layer thicknesses for this structure were 20.5 Å for InAs, and 24 Å for GaSb..	25
3.9 (200) dark-field images of short-period superlattice structures (SLS) with periods (a) 32Å, (b) 24Å, (c) 17Å and (d) 11Å. Inset in (d) is a low magnification image showing extensive disorder in the 11Å-SLS.....	27
3.10 (200) dark-field images showing (a) a 17Å –SLS grown with GaSb growth rate of1Å/s, and (b) a similar structure grown with a GaSb growth rate 0.5Å/s.....	29
3.11 An AFM micrograph image of a region 2 m x 2 m area of the QD structure resulting from the combined InAs SAQD and subsequent GaSb deposition. The inset is the RHEED image down the (110) direction of the sample showing elongated features at the 3D diffraction locations....	32
3.12 Cross sectional (220) dark-field transmission electron microscope micrograph showing the internal structure (cross-section) of a surface HEQUAD. The InAs core (a) is seen as a semi-spherical cap above the GaAs substrate and the GaSb crowns (b) the InAs.....	34
3.13 XEDS spectrum taken from various regions in the quantum dot structure.....	36

SUMMARY

In this report we describe results from transmission electron microscope (TEM) studies on a variety of III-V semiconductor thin films grown by molecular beam epitaxy (MBE). The various techniques employed in these studies include, high-resolution TEM (HRTEM) methods conventional bright and dark-field imaging, and X-ray energy dispersion spectrometry (XEDS). The materials investigated include, short-period superlattices and novel heterojunction quantum dot structures based on the InAs-GaSb system. The important findings in these studies may be summarized as follows:

1. Employing the focal-series reconstruction technique in HRTEM, we have developed a new method for true atomic scale quantitative chemical mapping of interfaces in mixed cation and anion III-V semiconductor heterostructures. Using this approach it was possible to independently determine changes in the In-Ga and As-Sb contents across ultra thin interfacial regions (~0.6 nm in width) in a InAs/InGaSb superlattice structure. A comparison of the cation and anion sublattice images revealed that intermixing at the InGaSb-on-InAs interface is confined to the In-Ga sublattice. Also, atomic scale roughness within the As-Sb sublattice of the InAs-on-InGaSb interface was discerned. This approach is general, permitting atomic-scale compositional analysis of heterointerfaces with two species per sublattice.
2. TEM studies were performed on several MBE grown short-period superlattices (SLS) with periods ranging from 50Å - 11Å. A gradual degradation in the structural quality occurred with reduction in the superlattice period, with its onset detectable in the 24Å-SLS and most significant in the SLS with period 17Å (superlattices with periods 30Å and higher exhibited good structural quality). The intended 11Å-SLS was mostly disordered although a superlattice structure was observed at isolated regions in the sample. It was possible to achieve significant improvement in structural quality even in the lower period SLS (nominally 16Å) when the GaSb growth rate was reduced from 1Å/s to 0.5Å/s.
3. We have demonstrated the fabrication of a self-assembled heterojunction quantum dot (HeQuaD) structure composed of multiple materials. This structure consists of a composite dot formed of an initial core of one material which results from normal self-assembly, followed by the epitaxy of a crown composed of a similarly strained material. Finally the entire dot structure is capped with a barrier material closely lattice matched to the substrate. In this demonstration, self-assembled InAs QDs were first formed on a GaAs substrate and subsequently crowned with GaSb. The entire structure was encapsulated with a GaAs cap layer. Atomic Force

Microscopy shows additional nucleation between the InAs layers has been minimized and cross-sectional transmission electron microscopy shows the formation of the composite structure

CHAPTER 1 INTRODUCTION

Artificially layered III-V structures grown by epitaxial techniques such as molecular beam epitaxy (MBE) and metal organic chemical vapor deposition (MOCVD) are important materials for optoelectronic applications. Examples of such materials include AlGaAs/GaAs and InGaAs/GaAs heterostructures, used in high electron mobility transistors [1] and lasers [2]. More recently, heterostructures containing combinations of arsenides and antimonides are of interest for number applications, including long-wavelength infrared detectors [3], infrared lasers [4], field effect transistors [5], resonant tunneling diodes [6]. Materials for many of these applications involve extremely thin layers requiring precise control of both thickness and composition of the constituent layers. From a microstructural perspective the important factors which determine high-quality material include layer thickness, interface abruptness, layer composition, and the composition modulation within each layer (as in graded $\text{Al}_x\text{Ga}_{(1-x)}\text{As}$ layers for photo refractive applications). In addition, structural defects, such as dislocations and stacking faults, arising from factors related to growth conditions or strain relaxation also play a critical role in the application of these materials.

The past two decades have witnessed significant developments in the application of transmission electron microscopy (TEM) for the routine analysis of III-V semiconductor heterostructures. In particular, high-resolution techniques have been developed to characterize III-V heterostructure interfaces at the atomic level [7-11]. In this study we apply cross-sectional TEM techniques, involving conventional bright-field and dark-field imaging, high-resolution TEM (HRTEM) and analytical electron microscopy (AEM), to characterize a variety of III-V semiconductor thin films. The materials investigated include superlattices based on the InAs-GaSb system and novel self-assembled quantum dot structures, all of which were grown by MBE. Furthermore, a new approach to quantifying the stoichiometry interfaces at atomic resolution is also developed.

CHAPTER 2

EXPERIMENTAL PROCEDURE

The theoretical concepts underlying the application of TEM for imaging of III-V semiconductor systems have been described in detail in the earlier reports [12, 13]. Briefly, we use the (200) dark-field imaging condition to maximize image contrast arising from the individual layers in the superlattice /heterostructure. The two-beam bright-field imaging condition with the diffraction vector (denoted \mathbf{g}) along $<200>$ and $<220>$ are used to image defects in the structure. The procedure for obtaining these imaging conditions are described in standard text books on transmission electron microscopy [14]. For the sake of continuity the procedures for performing the HRTEM experiments are described in Chapter 3.2, along with methods employed for performing the data analysis.

Samples for TEM observations was performed by Ar^+ ion-milling at 5 keV with liquid nitrogen cooling until perforation and subsequent cleaning at 3 keV to minimize the thickness of the amorphous surface layer induced by the milling process. In the XEDS experiments samples were also prepared by the small angle cleavage technique. TEM observations were performed using a Philips-CM 200 FEG transmission electron microscope equipped with a field emission gun, operated at an accelerating voltage of 200 kV.

CHAPTER 3

RESULTS AND DISCUSSION

3.1 Quantifying Stoichiometry of III-V Semiconductor Interfaces

The main objective of this section is to describe an approach for compositional analysis of ultra thin interfaces (around 1 nm) in InAs-GaSb superlattices at atomic spatial resolution. In the past decade several approaches based on high-resolution transmission electron microscopy (HRTEM) have been developed for compositional analysis of III-V semiconductor interfaces [7,8,10,11]. However, the techniques employed to obtain the compositional information restricts their application to ternary III-V systems (such as GaAs-AlGaAs). Furthermore, the resolution of these techniques is limited to the point-resolution of the microscope, which typically ranges from 1.7 Å to 2.5Å for mid-voltage TEMs. More recently, significant experimental and computational advancements have been made in HRTEM-based techniques designed to retrieve the electron wave function at the exit surface of the specimen [15-17]. The use of exit-plane wave function (EPWF) images offers important advantages over existing methods. First, the attainable resolution is closer to information limit of the microscope, which for modern field-emission gun transmission electron microscopes (FEGTEM) can be around 1Å or lower; this would permit an independent analysis of both group-III and group-V sublattices. Second, imaging artifacts due to contrast delocalization and other aberrations arising from the objective lens, invariably present in normal HRTEM images, can be corrected. In this work we employ the focal-series reconstruction technique to investigate the applicability of EPWF images for an atomic-level quantitative mapping of stoichiometry across III-V semiconductor interfaces. The results from this study show that the phase-component of the EPWF images (hereafter referred to as “EPWF-phase images”) clearly reveal changes in stoichiometry across interfaces at atomic resolution. The method of factorial analysis of correspondence (FAC) is used to extract the compositional profile representing the observed changes in stoichiometry.

Two samples were investigated in the present study. One was a $\text{Al}_x\text{Ga}_{(1-x)}\text{As}/\text{GaAs}$ multiple quantum well heterostructure grown on a (100)-GaAs substrate by molecular beam epitaxy (MBE). The nominal thickness for the GaAs quantum wells and the $\text{Al}_x\text{Ga}_{(1-x)}\text{As}$ barriers were 28Å (approx. 10 ML) and 200 Å (70 ML), respectively. The nominal composition of the $\text{Al}_x\text{Ga}_{(1-x)}\text{As}$ layers was $x_{\text{Al}} = 0.5$. The second sample investigated was a $\text{In}_x\text{Ga}_{(1-x)}\text{Sb}/\text{InAs}$ superlattice structure grown on a (100)-GaSb substrate by MBE, consisting of alternating layers of $\text{In}_x\text{Ga}_{(1-x)}\text{Sb}$ and InAs layers with a nominal period of 73Å. The intended layer thickness for InAs and $\text{In}_x\text{Ga}_{(1-x)}\text{Sb}$ layers were 6.5 ML (approx. 20Å) and 17.5 ML (approx. 53Å), respectively. The nominal composition of the $\text{In}_x\text{Ga}_{(1-x)}\text{Sb}$ layers was $x_{\text{In}} = 0.25$. Following previous studies [7,8] the interfaces were imaged along the <001> projection, to exploit both the contributions from the four

“chemically sensitive” (200) reflections. Samples for HRTEM observations were prepared by mechanical grinding followed by ion-milling to perforation with Argon ions at an accelerating voltage of 5kV. To reduce milling induced surface roughness the further milling was performed at 3kV, which was then followed by final polishing at 1kV. The entire milling process was performed with the samples mounted on a liquid-N₂ cooled cryostage.

The HRTEM observations were performed using the Philips CM300 FEG/UT TEM located at the National Center for Electron Microscopy, Berkeley, CA. A detail report describing the experimental set-up to perform the focus variation technique using this TEM has been published previously [21,22]. In these studies the resolution achievable upon implementing the focus variation technique was demonstrated to be 0.85 Å. In the present study, a through focus series of 20 HRTEM images was digitally acquired at equally spaced defocus values, starting at an underfocus value of -270 nm and a focal increment step of 2 nm. The images were recorded using a 2048x2048 slow-scan charge-coupled device (CCD) camera with a Gatan Image Filter (GIF) attachment at a spatial sampling rate of 0.021 nm/pixel. Using low magnification on-axis bright field imaging condition the investigations were confined to regions within the first minimum in the observed thickness fringes. Based on image dynamical diffraction calculations employing the multislice algorithm [23] we estimate the thickness to be in the range of 50Å -80Å.

The numerical reconstruction procedure was performed using the software TruelImage [24], which is the commercial version of the Philips/Brite-Euram focal series reconstruction package developed by Coene and Thust [16, 17]. The TruelImage software package also includes a module for correcting residual aberrations due to coma, two-fold and three-fold astigmatism. Prior to reconstruction, a noise reduction procedure employing the background subtraction filter [25] was applied to the digitally acquired HRTEM images. We note that performing the reconstruction using the as-acquired HRTEM images and then applying the noise reduction procedure on the EPWF images yielded similar results. However, we observed that performing the noise reduction on the HRTEM images yielded better convergence in the calculated EPWF images, and further, better agreement between experimental images and images simulated based on the calculated EPWF images. Also, it was easier to perform the posteriori aberration correction with the EPWF images retrieved from the noise reduced HRTEM images.

Figure 1 (a) is a EPWF-phase image of a GaAs quantum well with the adjacent AlGaAs barriers, wherein the magnitude of the phase at the atomic positions in the AlGaAs region can be used to identify the group-III (Al/Ga) and group-V (As) sublattices in the entire image. Based on image simulations performed for AlGaAs we observe that the positions with lower magnitude in phase correspond to the group-III (Al/Ga) sublattice. Figure 1(b) shows a plot of a

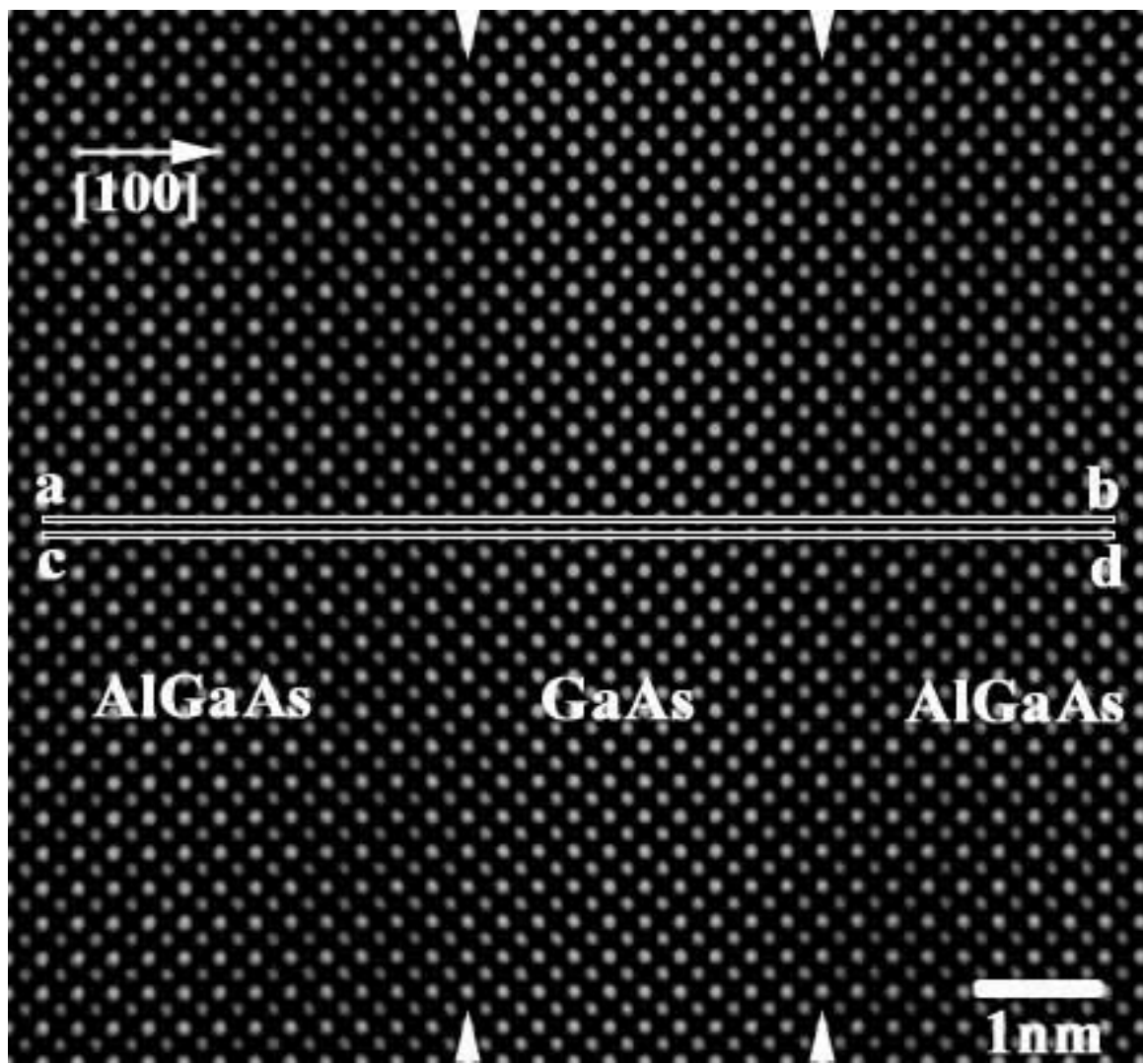


Fig. 1 (a)

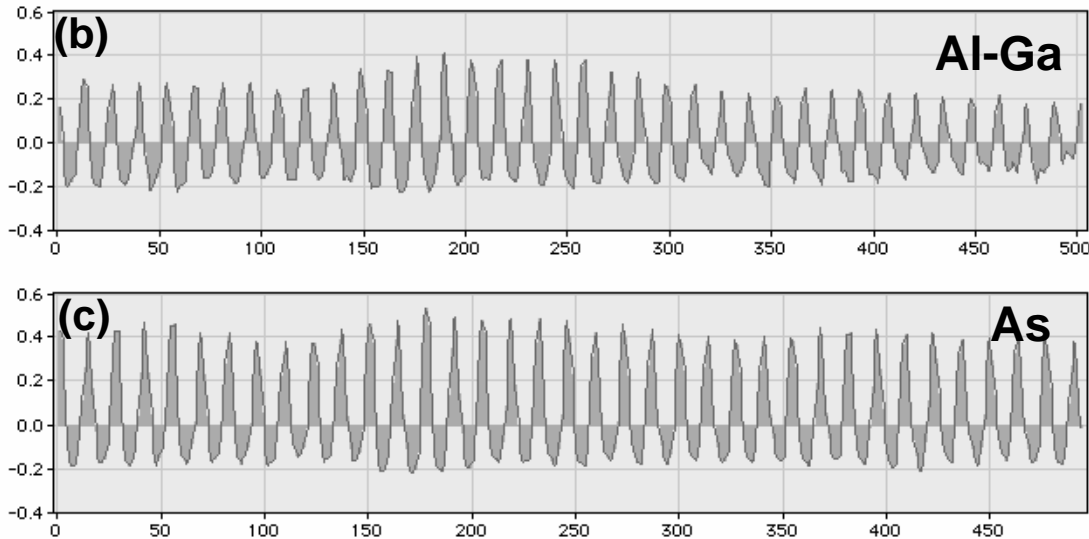


Figure 1. (a) Reconstructed phase image of $\text{Al}_{0.6}\text{Ga}_{0.4}\text{As}/\text{GaAs}$ interfaces, where the position of each interface is denoted by an arrow, (b) profile along Al-Ga sites, denoted by line a-b, and (c) profile along the As sites, denoted by line c-d.

line scan along the Al/Ga sublattice, denoted by line AB in Fig. 1(a). A systematic variation in phase magnitude is observed across the GaAs-on-Al_xGa_(1-x)As and the Al_xGa_(1-x)As-on-GaAs interfaces. On the other hand, as shown in Fig. 1(c), an almost constant value is observed across both interfaces for a line scan along the adjacent As sites, denoted by line CD in Fig. 1(a). These observations are consistent with a grading in the Al/Ga composition at each interface.

Figure 2(a) is a EPWF-phase image showing an InAs/In_{0.25}Ga_{0.75}Sb/InAs structure, wherein the interface positions are clearly identified by the distinct shift in the intensity-maxima to the “heavier” atomic column, i.e. In sites in the InAs region and Sb sites in the InGaSb region. The line scans across the interfaces along adjacent group-III (denoted by line AB) and group-V sublattices (denoted by line CD) are shown in figs. 2(b) and 2(c), respectively. The plots clearly reveal changes in the In/Ga and As/Sb contents across the interfaces. It is interesting to note the presence of interfacial regions about 2 ML (about 6 Å) in width, in the vicinity of the InGaSb-on-InAs and InAs-on-InGaSb interfaces. A qualitative inspection of the line profiles along the group-III and group-V sites within this region reveals, that the interfacial region in the vicinity InGaSb-on-InAs interface is In_xGa_(1-x)As-like. The interfacial region near the InAs-on-InGaSb interface corresponds to those sites exhibiting asymmetry in the As/Sb profile shown in Fig. 2(c). These observations are consistent with the presence of a Ga-to-In exchange at the InGaSb-on-InAs interface and an As-to-Sb exchange at the

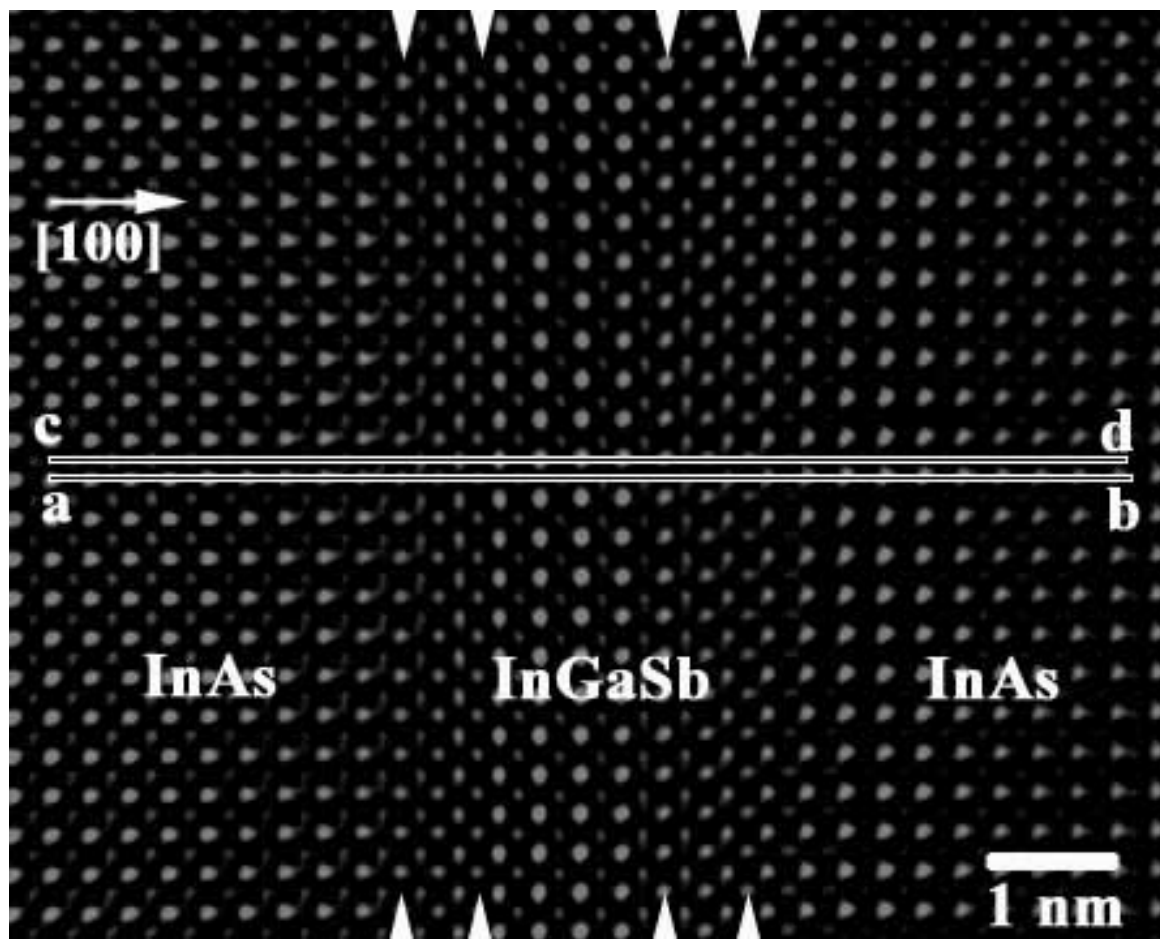


Fig. 2 (a)

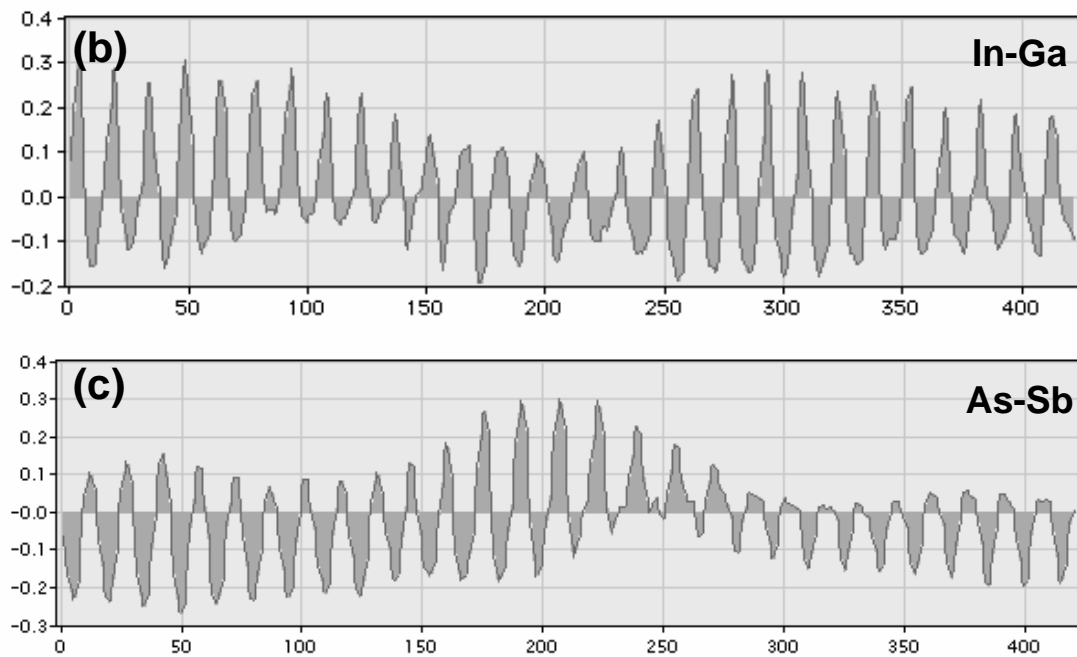


Figure 2. (a) Reconstructed phase image of $\text{In}_{0.25}\text{Ga}_{0.75}\text{Sb}/\text{InAs}$ interfaces, where the position of each interface is denoted by an arrow, (b) profile along In-Ga sites, denoted by line a-b, and (c) profile along the As-Sb sites, denoted by line c-d.

InAs-on-InGaSb interface. Evidence for such reactions have been reported in in-situ desorption mass spectrometry experiments [26].

To confirm that the observed changes in phase magnitudes across interfaces indeed relate to changes in interfacial stoichiometry, and further, to quantify this relationship, an image simulation study was performed on an AlGaAs/GaAs model structure. The model consisted of a GaAs layer of thickness 8 ML in between $\text{Al}_{0.4}\text{Ga}_{0.6}\text{As}$ barriers with a graded interface on side and an abrupt interface on the other. The change in Al/Ga compositions for the graded interface was set to be linear with width of 3 ML and $x_{\text{Al}/\text{Ga}}$ varying from 0.1 on the GaAs-side to 0.3 on the $\text{Al}_{0.4}\text{Ga}_{0.6}\text{As}$ -side. Image simulations were performed to calculate EPWF images for sample thickness ranging from 30-70 Å. The HRTEM thru-focus images for settings used in experiment were computed based on the quasi-coherent approximation for beam-divergence and chromatic aberrations [23]. Reconstructions were performed on the simulated HRTEM image series to retrieve the EPWF image of the model structure.

In addition to the image simulation procedure a suitable method for quantifying the information in the phase images is also needed. While integrated intensities within each unit cell would suffice for the analysis of the (noise free) simulated images, a more reliable technique, which is robust to the noise levels present in experimental images, is required. In the present study we employ the method of FAC, which has previously been used for the analysis of conventional HRTEM images of interfaces in GaAs/AlGaAs heterostructures [27] and precipitate/matrix (γ/γ) interfaces in Ni alloys [28].

A detailed discussion on FAC approach for analysis of HRTEM images has been described elsewhere [28-30], only a brief description of calculations pertaining to the images investigated in this study is presented. The entire image is first subdivided into unit cells of size 2.8Åx2.8Å digitized to $n \times n$ pixels, such that the As atoms are located at the corners and the Al/Ga atoms at the center. Then unit cells within a rectangular strip of width 1 unit cell parallel to the interface and height normal to the interface are extracted. The height of the rectangular region is chosen such that it spans several unit cells on either side of both interfaces. The two dimensional unit cells are then converted to vectors of size $p=n^2$, and a data matrix D is constructed with the individual images being either the row or column vector of the matrix. A variance-covariance matrix (S), representing the correlations between the different image, is then constructed after appropriate normalization and transposition operations performed on D. A diagonalization is then performed on S to yield eigenvalues λ_α (with a trivial eigenvalue of $\lambda_1=1$) and their corresponding eigenvectors v_α . The magnitude of λ_α (excluding λ_1) is an indicator of the relative importance of the corresponding eigenvector to the original data. The trends in a given set of images can be extracted by examining the projections C_α of each image on the corresponding

eigenvectors v_α , where C_1 is the projection on the first (trivial) eigenvector v_1 , and C_2, C_3 , etc., are the projections on subsequent (non-trivial) eigenvectors. A flow chart depicting the different steps in performed in the FAC procedure is presented in Fig. 3.

Application of FAC to the simulated EPWF-phase image of the model structure shown in Fig. 4(a) yielded an eigenvector, which accounted for 97% of the observed variance. A plot of the coefficients C_1 obtained by the projection of the extracted unit cell on to this eigenvector is presented in fig. 4(b). It is clear that the variation in C_1 across the interface mimics the composition profile in the model structure (denoted “Model”). A good agreement in composition profile is also observed for the reconstructed EPWF-phase images obtained by applying the focal series reconstruction (FSR) package to the simulated HRTEM thru-focus images (denoted “Model +FSR”). Image simulations were also performed to examine the effects of the amorphous surface layers. The amorphous layers were modeled using atom-displacement, atom-density and layer thickness as free parameters [31]. Since varied results were obtained depending on the values for the different parameters, they were adjusted by trial and error so as yield results such that the standard deviations for C_1 in the AlGaAs and GaAs regions were similar to those observed in experiments (see later). Again, HRTEM images for a model combining an amorphous layer of thickness 12 Å with the model structure were computed and subsequently reconstructions were

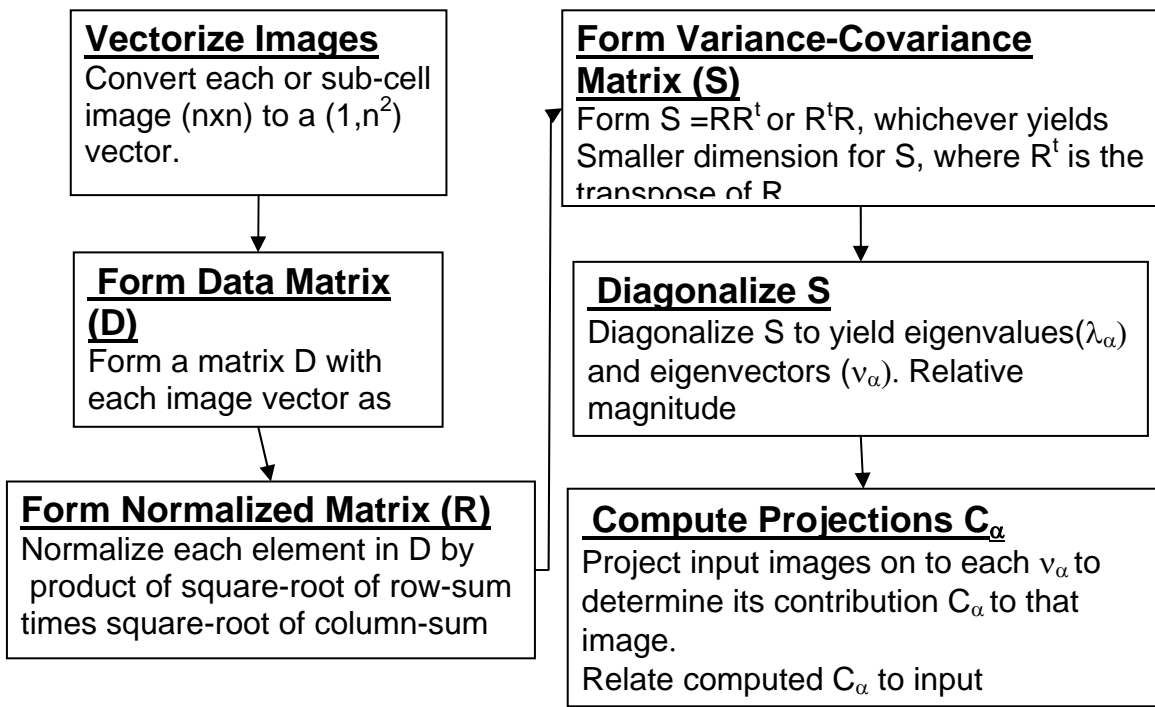
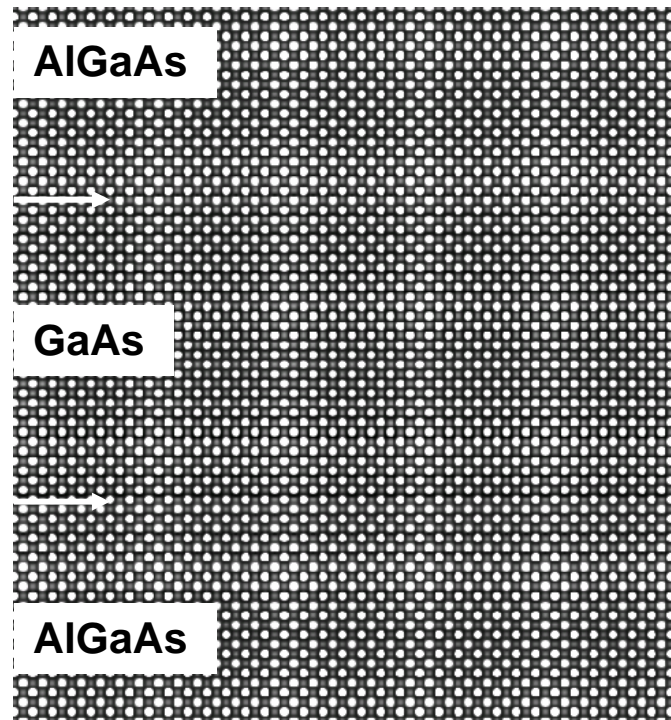


Figure 3. Flow chart describing the different steps employed in the factor analysis procedure.



(a)

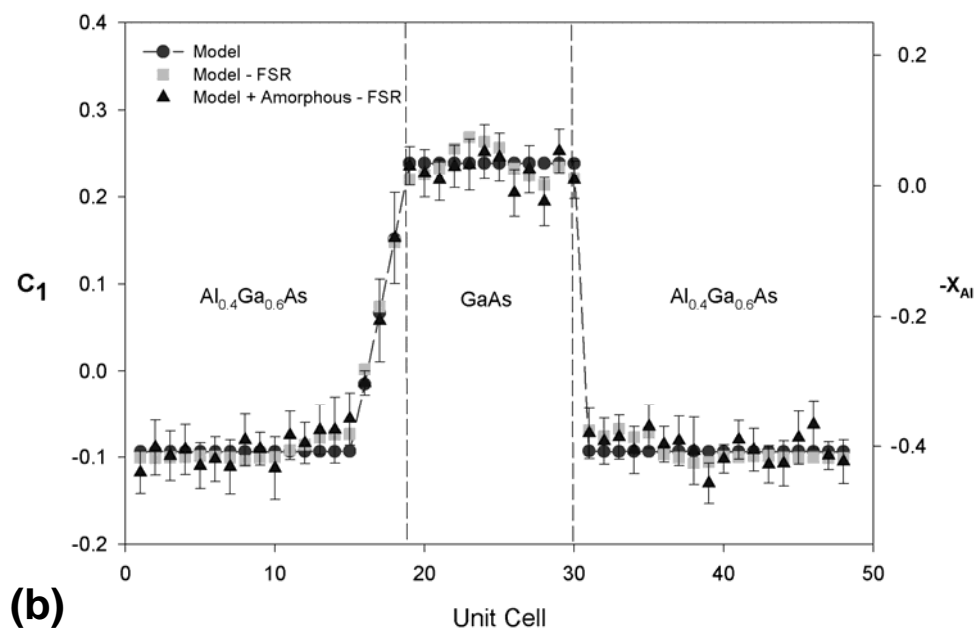


Figure 4. (a) A simulated EPWF-phase image of a $\text{Al}_{0.4}\text{Ga}_{0.6}\text{As}/\text{GaAs}/\text{Al}_{0.4}\text{Ga}_{0.6}\text{As}$ model structure with an abrupt interface and a graded interface and (b) a plot of C_1 for each unit cell across the interface calculated for specimen thickness of 6.7nm.

performed to obtain the EPWF image. As shown in Fig. 4(b), the results obtained upon performing the FAC procedure on the reconstructed EPWF-phase images are in excellent agreement with input composition profiles (denoted “Model+FSR+Amorphous”).

The image simulation study performed for the AlGaAs/GaAs structure was repeated for a $\text{In}_{0.25}\text{Ga}_{0.75}\text{Sb}/\text{InAs}$ structure, with the graded interfaces having linear variations in both In/Ga and Sb/As sublattices. For simplicity strain was not included in the calculation. Since choice of the unit cell employed in the AlGaAs/GaAs case is not applicable due intermixing is present in both sublattices, the analysis was performed by first dividing this unit cell into sub-cells with only the group-III or group-V atomic columns at the center and then applying the FAC procedure independently to each sublattice. The results presented in Fig. 5 show good agreement with the C_1 calculated and the model profiles. An important result obtained for both systems investigated in this study is the linear dependence of C_1 on composition. This indicates that at a constant thickness the change in phase at an atomic column associated with replacement of one atomic species by another is linear. Although this conclusion is based on ignoring lattice strain, we believe that to a large extent its effect would only be to affect the spatial position of the phase maxima and not their magnitude.

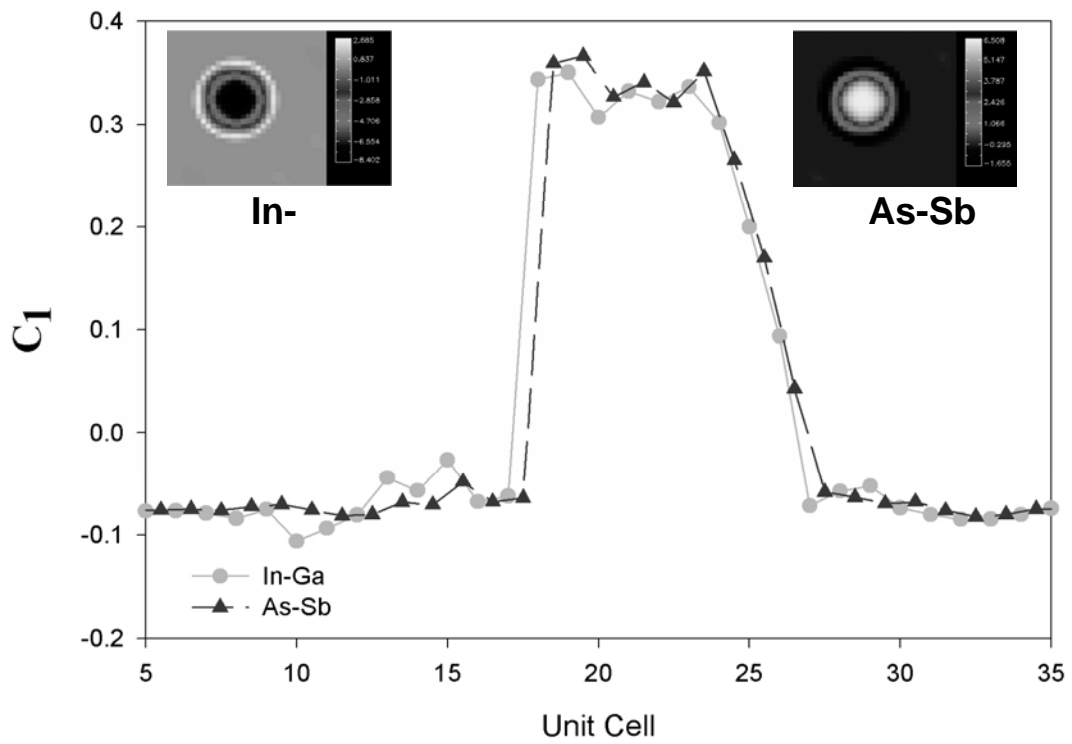


Figure 5 A plot showing the variation of C_1 for an InAs/ $\text{In}_{0.25}\text{Ga}_{0.77}\text{Sb}$ model structure with an abrupt interface on one side and a linear grading in both the In/Ga and As/Sb sublattices on the other, for a specimen thickness of 6nm. The inset shows the eigenvector images for the In-Ga and the As-Sb sublattices onto which each unit cell was projected to obtain C_1 .

The results on applying the FAC to the experimental EPWF-phase images are shown in Figs. 6(a), 7(a) and (b). The color maps denote the magnitude of C_1 determined for each unit cell. The average thickness of the GaAs and InGaSb layers are good agreement with their respective nominal values. The variations in the color shades away from the interface capture the degradation in quality of images due to noise arising from surface roughness due to ion-milling and beam irradiation. A compositional profile normal to the interface was obtained by computing the average values of C_1 along rows of unit cell parallel to the interface. The interfacial regions observed in Fig. 2(a) are also marked in Fig. 7(a) and (b). A comparison of the In/Ga (Fig. 7a) and As/Sb (Fig. 7b) maps confirms that the interfacial region near the InGaSb-on-InAs (bottom) interface is $\text{In}_x\text{Ga}_{(1-x)}\text{As}$ -like. It is also interesting to note that the As-sublattice in the InGaSb-on-InAs interface is compositionally more abrupt than its corresponding In-sublattice and both sublattices near the InAs-on-InGaSb interface. These observations are again consistent with the presence of the In-Ga and As-Sb exchange mechanisms referred to earlier. The values of C_1 were converted to composition assuming the nominal values of composition for unit cells well away from the interface. The results have been presented in Figs. 6(b)-7 (c). The error bars denote values of σ obtained for the corresponding row of unit cells.

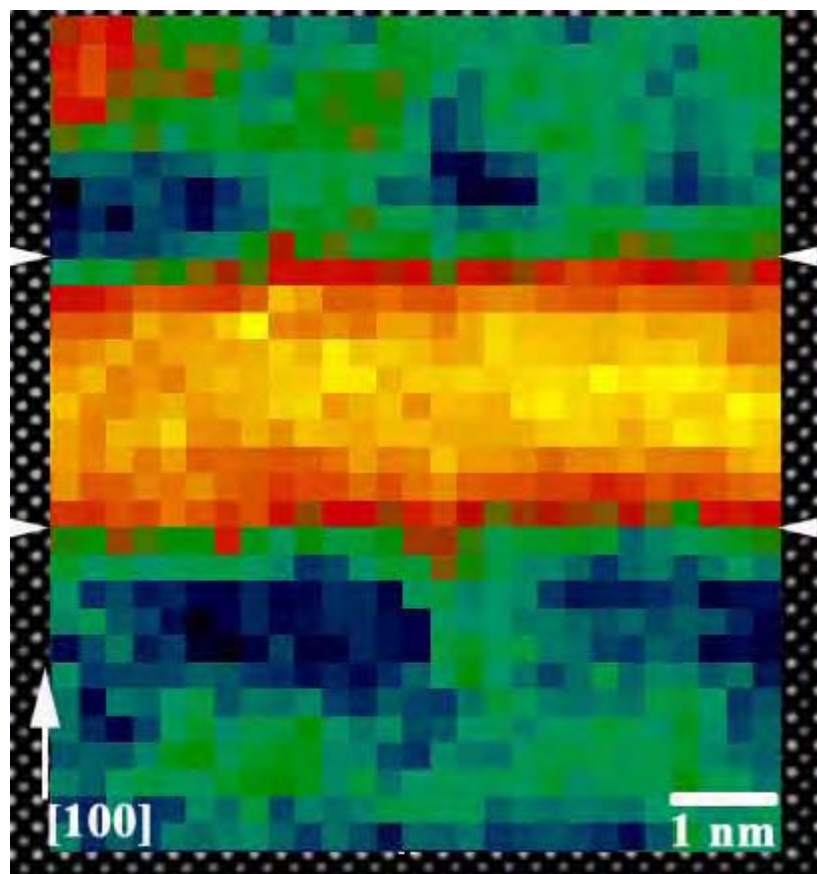


Figure 6 (a)

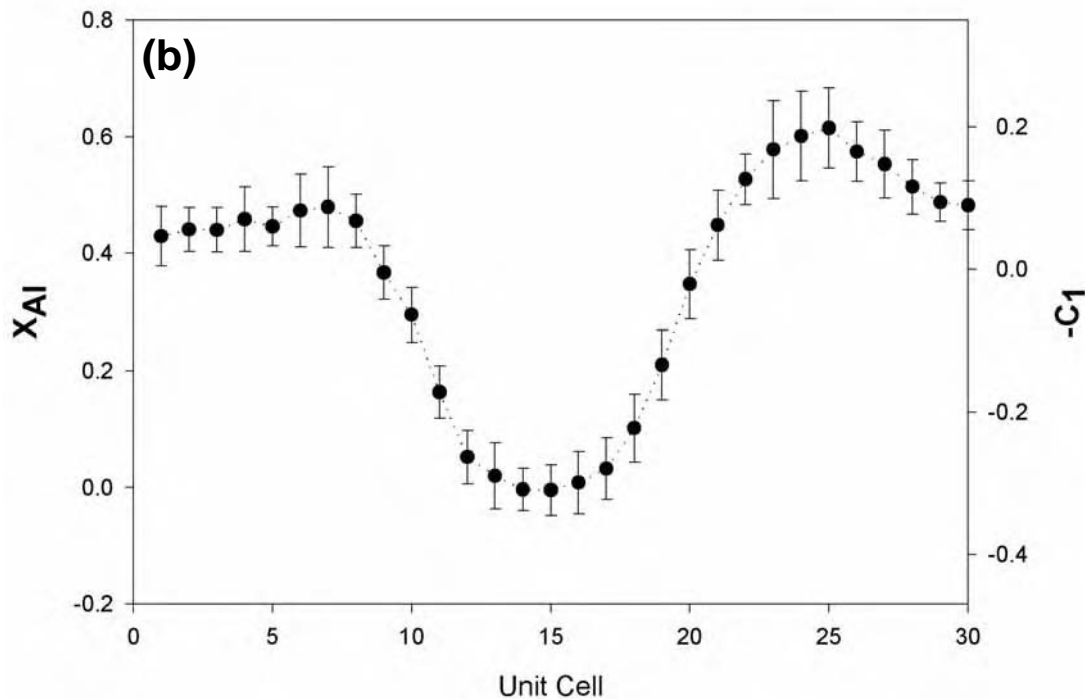
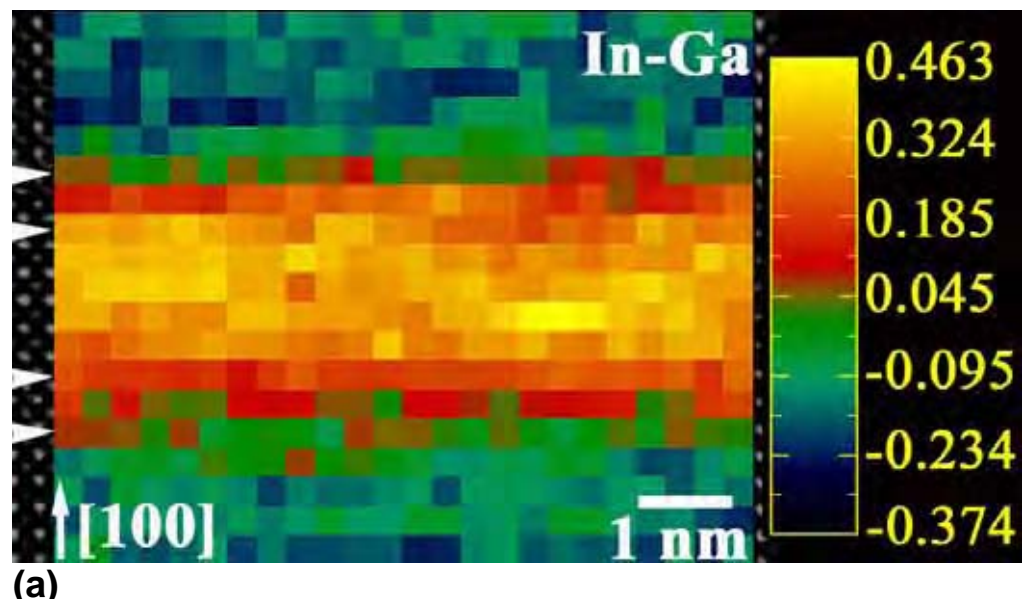


Figure 6 (a) Composition map showing variation of C_1 from the experimental EPWF-phase image for AlGaAs/GaAs interface shown in Fig. 1(a), and (b) profile of x_{Al} and C_1 normal to the interface and averaged over unit cells parallel to the interface.



(a)

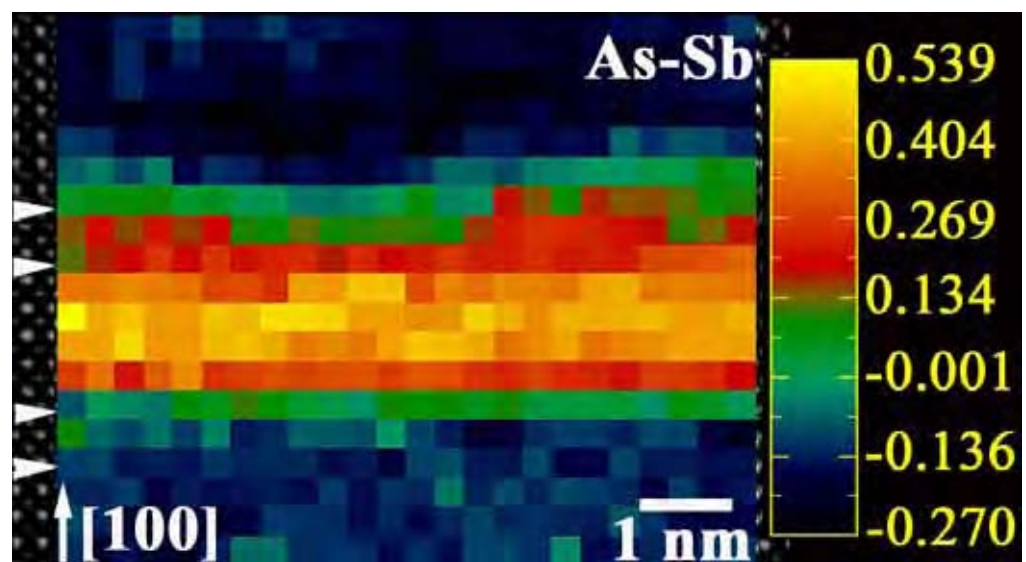


Figure 7

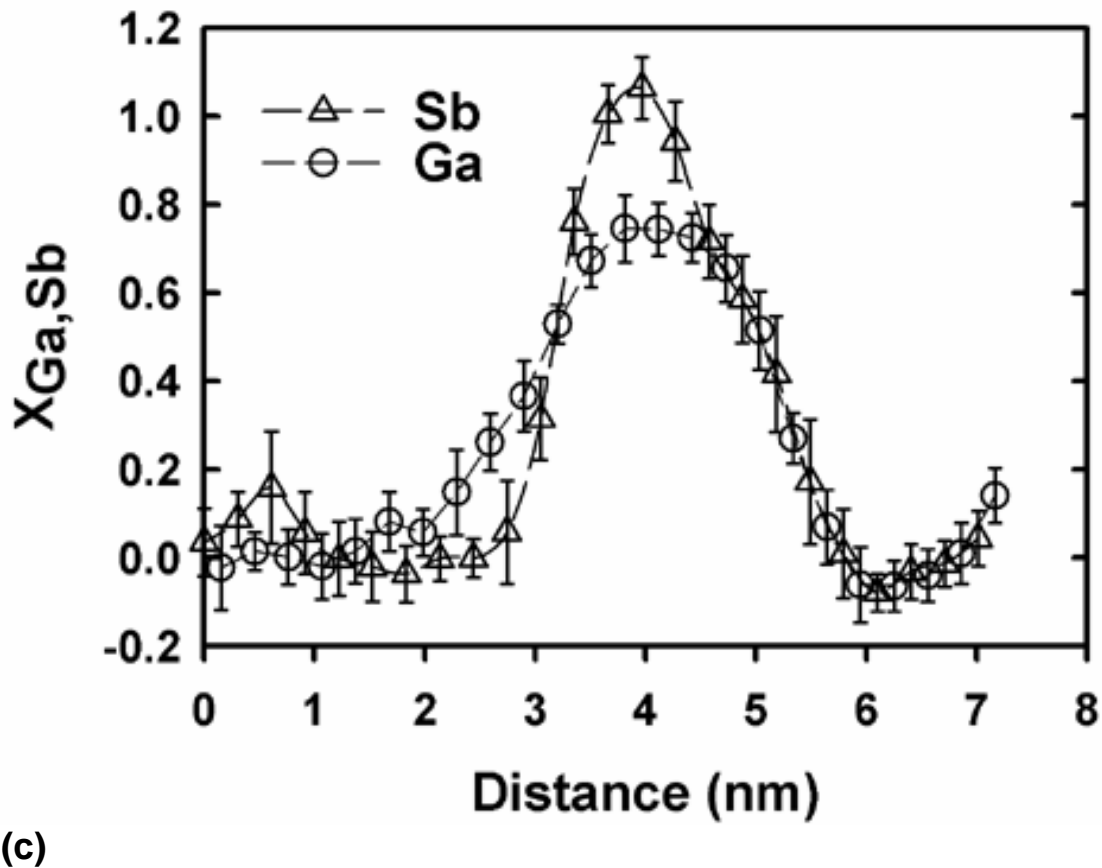


Figure 7 (a) Composition maps of the phase image in Fig. 2(a), showing the variation of the FAC coefficient C_1 within (a) the In-Ga sublattice and (b) the As-Sb sublattice. The arrows locate the interfacial regions in Fig. 2 (a), and (c) compositional profiles of the In-Ga and As-Sb sublattices showing the mean compositions, x_{Ga} and x_{Sb} , of each atomic layer along the [100] direction in Fig. 2(a)

It would be interesting to compare the results obtained for AlGaAs/GaAs system in this study with those reported in earlier studies. In one of the earliest studies by Ourmazd and co workers [7,8], a separation of 12σ between GaAs and AlGaAs of nominal $x_{Al}=0.4$ is reported, which corresponds to a sensitivity of $\Delta x_{Al} = 0.07$ at a 95% confidence level. In the present study, for an AlGaAs of composition $x_{Al}=0.5$ we obtained a separation from GaAs of about 9σ , which corresponds to a sensitivity of $\Delta x_{Al} = 0.11$. A similar analysis of the experimental data obtained for the InAs/InGaSb showed a separation of about 12σ the In/Ga sublattice and about 13σ , which correspond to a sensitivity of $\Delta x_{Ga}=0.13$ and $\Delta x_{Sb}=0.15$. The lower sensitivity in Δx_{Al} obtained in our study in comparison to the study by Ourmazd [13] can be attributed to two reasons: (1) the samples were prepared by ion-milling whereas the previous work employed chemical etching. This study specifically mentions that the noise levels in images of samples prepared from ion milling was significantly higher, yielding a separation of only 5σ , and (2) the sample thickness from which the images were obtained was significantly higher (170 \AA) than in the present study (70\AA). In the present case the fraction of the contribution from the crystalline portion of the sample is lower than in the earlier study. These considerations indicate that in the present technique sensitivity can be increased with further improvement in sample preparation procedures.

Finally, we emphasize the generality of the present approach. Previous methods are based on the dynamical behavior of either the chemically sensitive reflections (such as the (200) and (420)) alone [7-9], or the combination of both chemical and structural reflection [10, 11]. These approaches require optimum settings for sample thickness and imaging conditions, which depend on the system being investigated. In the present study, the choice of sample thickness, independent of the material system, is typically confined to $30\text{-}60 \text{ \AA}$ to satisfy assumptions made in calculating the non-linear interactions between diffracted beams in the reconstruction procedure. The choice of imaging conditions, viz. the starting defocus and the defocus step size used to obtain the thru focal series, is dependent either on the resolution achievable by the microscope or the resolution intended for performing the analysis. Although this method has been demonstrated for interfaces in III-V semiconductor systems, the technique is sufficiently general to be applicable to other material systems, especially in the area of nanotechnology, where interfaces are known to play a prominent role.

3.2 TEM of InAs/GaSb Short-Period Superlattices

In this section we describe TEM characterization studies performed on short-period InAs/GaSb superlattices which were designed for infrared detection in the mid-IR ($3\text{-}5 \mu\text{m}$) region. These studies highlight the dependence of structural quality on the superlattice period (particularly when the individual layers are only a few monolayers in thickness) and its optimization through proper

choice of growth conditions. The superlattice structures (SLS) examined in this study were all grown by molecular beam epitaxy on (100)-GaSb substrates. The superlattice period ranged from 44 Å to 11 Å. Figure 8 (a) is a (200) dark-field image of a 44Å-SLS wherein the InAs (dark) and GaSb (bright) are clearly distinguished. Figure 8(b) is a high-resolution transmission electron microscope (HRTEM) image of the SL structure showing the individual layers of InAs and GaSb, with well-defined interfaces. The position of each interface is identified by observing the distinct shift in the bright and dark dots between the individual layers. Detailed examination of several such regions revealed that the transition from one layer to another occurred within 1-2 ML, thereby indicating both the high quality and the uniformity of the interfaces within the SLS.

Figure 9 (a-d) shows (200) dark-field image of the SLS with periods 32 Å, 24 Å, 17Å and 11 Å. where the evolution of the overall microstructure with reduction in the SL is clearly revealed. It is observed that the 32Å-SLS (Fig. 9(a)) is similar to the 44Å-SLS (Fig. 8) exhibiting uniformly thick layers with smooth and abrupt interfaces. With reduction in the SLS period to 24 Å (see Fig. 9(b)), slight undulations in the individual layer thickness are observed. Further reduction in the SLS-period to 17Å results in significant structural degradation, which is characterized by noticeable interfacial roughness and modulations in contrast within each layer. Finally, for the smallest SLS period (11Å) in the series

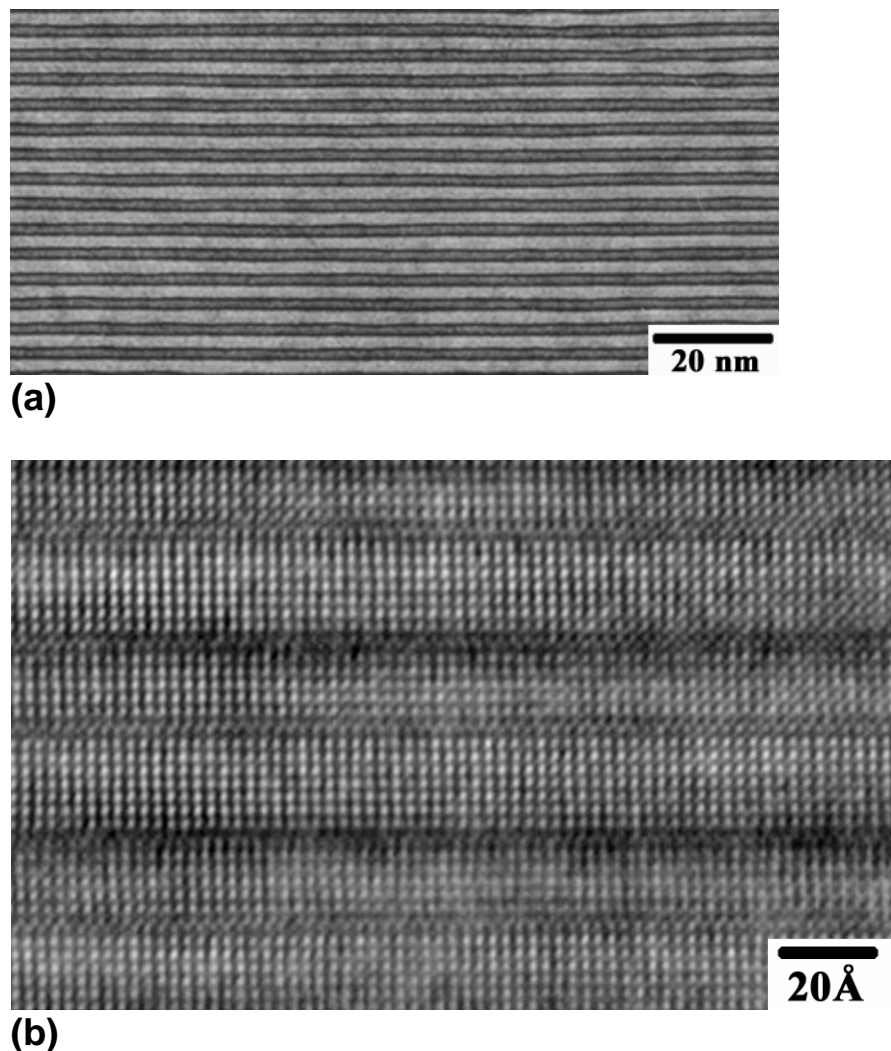
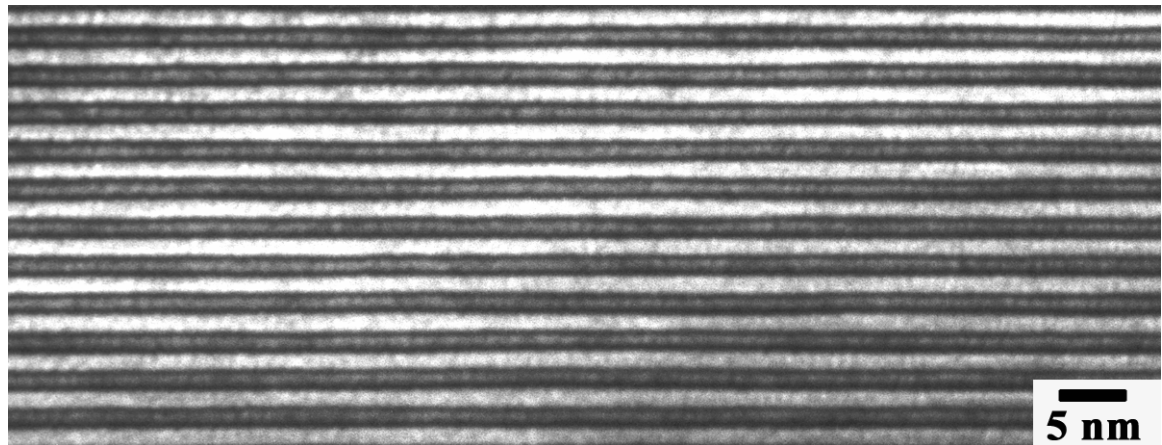
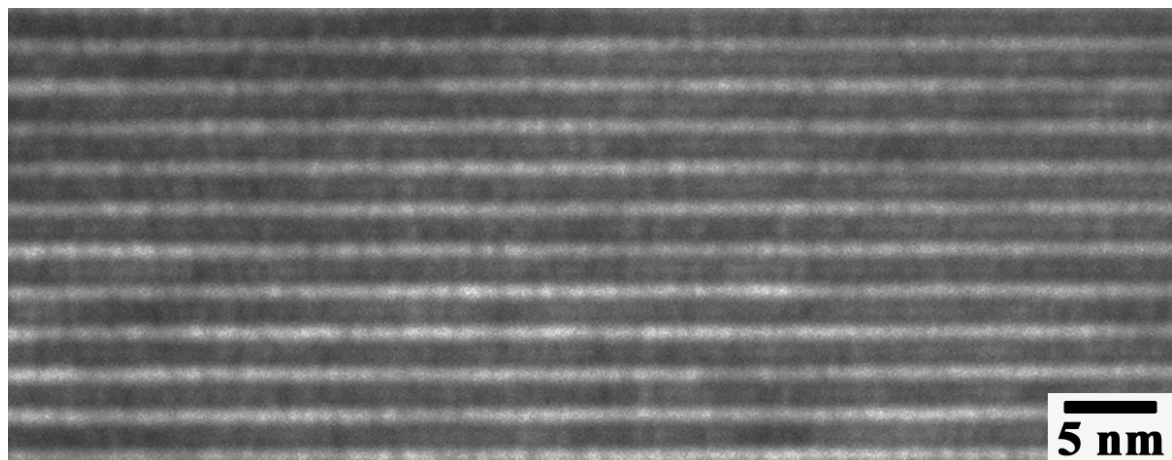


Figure 8 (a) A (200) dark-field image and (b) a [010] cross-sectional HRTEM image of an InAs-GaSb superlattice structure showing smooth and abrupt interfaces between the individual layers. The intended individual layer thicknesses for this structure were 20.5 Å for InAs, and 24 Å for GaSb.

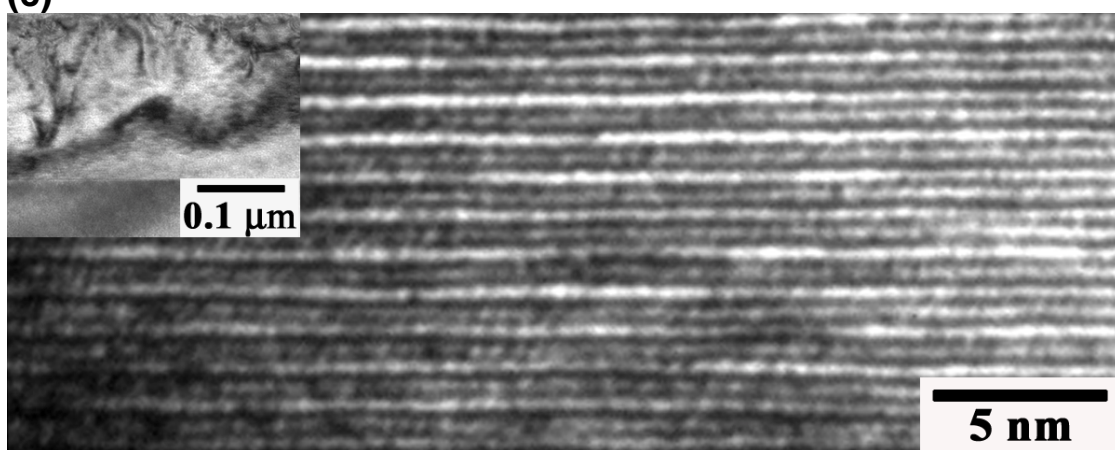
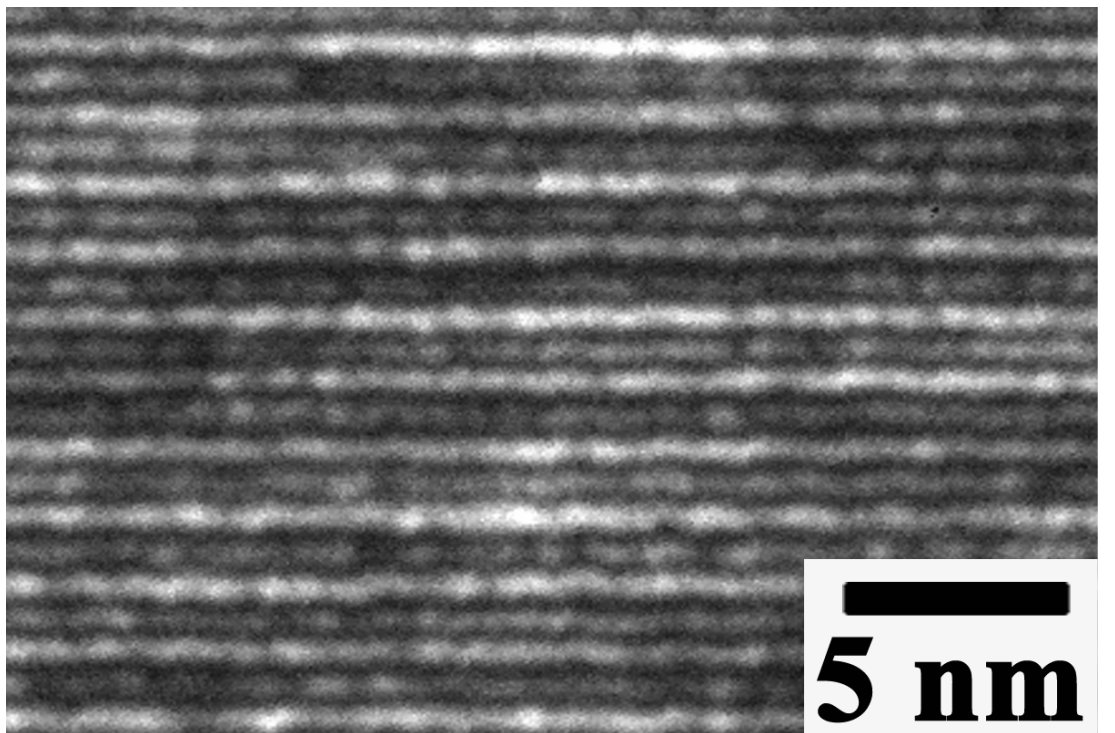


(a)



(b)

Figure 9



(d)

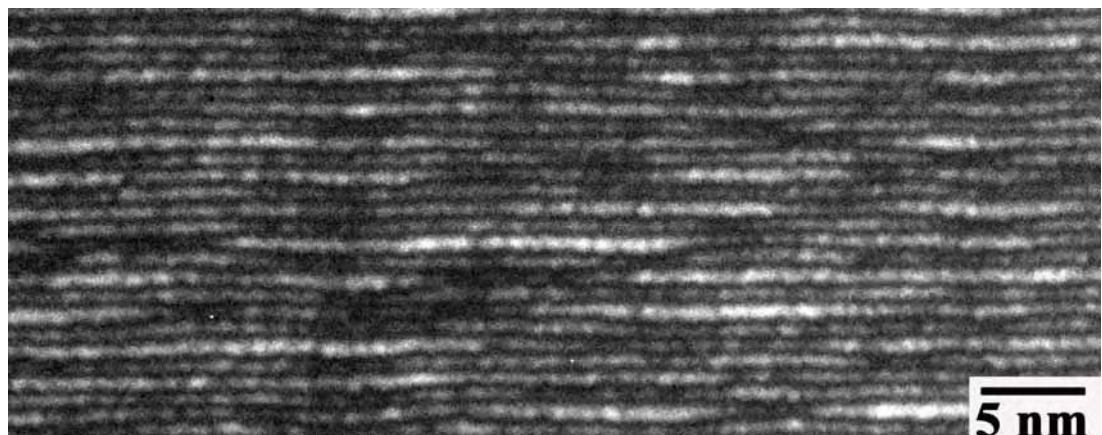
Figure 9 (200) dark-field images of short-period superlattice structures (SLS) with periods (a) 32 Å, (b) 24 Å, (c) 17 Å and (d) 11 Å. Inset in (d) is a low magnification image showing extensive disorder in the 11 Å-SLS.

it is observed that the microstructure is mostly disordered (see inset in Fig. 9(d)), although the SLS was preserved in isolated regions, as noted in Fig. (9d).

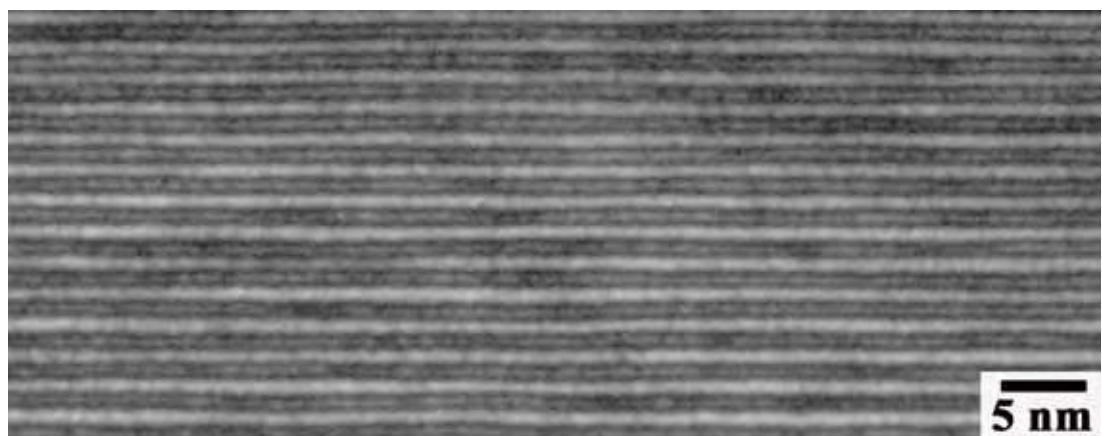
The above analysis suggests that in order to realize higher quality structure in the thinner SLS, better layer control is required. To achieve this, two 17Å-SLS were grown using different GaSb growth rates (1.0 and 0.5 Å) with no intentional interface control. The InAs growth rate for both samples was fixed at 0.3 Å/s. Figures 10 (a) and (b) are respectively (200) dark-field images of the two SLS grown with the higher and lower GaSb growth rate. It is clear that a dramatic improvement in the structural quality is obtained in samples grown with lower GaSb growth rate (Fig. 10 (b)).

3.3 TEM of Heterojunction Quantum Dot Structures

Quantum dots (QDs) have been the focus of considerable research (32-34) in part due to the unique properties, which arise from confinement of the electrons and holes in the region of the dot. QDs have been found to form during epitaxy through a Stranksi-Krastanov process in which a wetting layer is first formed. With additional growth QDs nucleate and grow on this layer. Research on this topic has found that the onset of nucleation required a critical coverage prior to QD formation. For self-assembly of InAs QDs on GaAs(001), the coverage is reported to be 1.6 monolayers. The number, spacing, size and geometry of the QDs have been found to be critically dependent on the growth



(a)



(b)

Figure 10 (200) dark-field images showing (a) a 17 Å –SLS grown with GaSb growth rate of 1 Å/s, and (b) a similar structure grown with a GaSb growth rate 0.5 Å/s.

condition [35]. These QDs have been vertically stacked due to a lowering in the nucleation barrier near the top of the dot [36]. Recently this effect has been used to stack GaSb dots on a buried InAs dot layer [37]. Although the InAs/GaAs epilayer-substrate pair has been the most extensively studied combination, similar results have also been found for most mismatched systems (33).

More recently, modification of the QD structure by changing the barrier material has been investigated. For example, InAs QDs have been formed on GaAs and capped with the growth of an InGaAs well layer, to produce a dot in a well structure (DWELL) [38]. This structure has the unique characteristic of increasing the capture of electron and holes initially by the well, which increases the likelihood of capture of the electrons, and holes by the QDs. The composition of the well structure has been shown to affect the quantum dot energy levels [39]. Finally, researchers have been adding an AlGaAs layer as the QD is capped. The composition of the AlGaAs and the location of this layer relative to the QDS modify the electron and hole levels. In this case certain energy levels may be affected more since the wavefunction is localized in particular regions of the dot and therefore may be selectively squeezed by the AlGaAs barrier.

The purpose of this work is to investigate the ability to grow a QD structure, which is composed of multiple materials through the self-assembly process in molecular beam epitaxy. In particular we demonstrate the ability to form self-assembled quantum dots that are composed of InAs and GaSb. We discuss this result in relation to nucleation theory and argue that it should be possible in large number of other material combinations.

All samples were grown in a GenII Varian MBE machine equipped with valved As and Sb crackers. The substrate was heated until the oxide thermally decomposed and 3D diffraction spots were visible in the RHEED pattern. A buffer layer was grown at rate approximately a 0.5 micron/hr with an As₂ equivalent flux of 6x10⁻⁶ torr for a time of 2 hours. The substrate temperature after oxide desorption and buffer growth was monitored by an IRCON Modline PLUS 'V' Series infrared pyrometer which detects radiation in a wavelength band of 0.91 - 0.97 micrometers. InAs self-assembled quantum dots (SAQDs) were grown at temperatures between 450°C and 525°C with an As₂ overpressure 2-8 x10⁻⁶ Torr. Subsequently GaSb was grown at similar temperatures and pressures in the range of 1.5-10 x10⁻⁷ Torr for various time periods. Samples were analyzed using a Park Scientific Autoprobe CP atomic force microscope using a combination of tapping and contact modes to eliminate artifacts.

Reflection high-energy electron diffraction (RHEED) was performed through out the self-assembly of the InAs QDs and the subsequent GaSb deposits. After a 1μm buffer layer growth, RHEED images down the 2x and 4x

direction of the As stabilized 2x4 reconstruction clearly showed a streaked surface. AFM analysis has shown we routinely achieve surfaces with 0.1-0.2 nm surface roughness. Approximately 3ML of InAs was deposited on the GaAs buffer layer. 3D diffraction was present indicating the formation of QDs. Evidence of 2D diffraction was still present indicating flat region between the QDs. The facets terminating the 3D InAs QD were exhibited as weak chevrons in the image located at the 3D diffraction spots. However the chevrons were not of sufficient quality to determine the facet planes present prior to growth of the GaSb [40]. GaSb was deposited on the InAs SAQDs.

Atomic force microscopy was performed on the combined InAs and GaSb QD structure. Figure 11 is an atomic force micrograph of the morphology over a 2 m x 2 m area showing that a QD structure is still present. These dots are elongated down the (110) direction. Line profiles of the dots indicate that the long dimension of the dot is 80nm and the short dimension is 40nm with a height of 15nm. This particular micrograph shows that reasonable uniformity is achievable in the formation of these QD structures. However, large variation in these structures was observed under different growth conditions. During the GaSb deposition, the RHEED pattern exhibited strong chevron features at the 3D locations. However the chevrons dramatically changed in shape from those typically observed during InAs SAQD growth to dashes seen in the inset in Figure 11 [41]. The removal of the original SAQDs feature suggests a change in

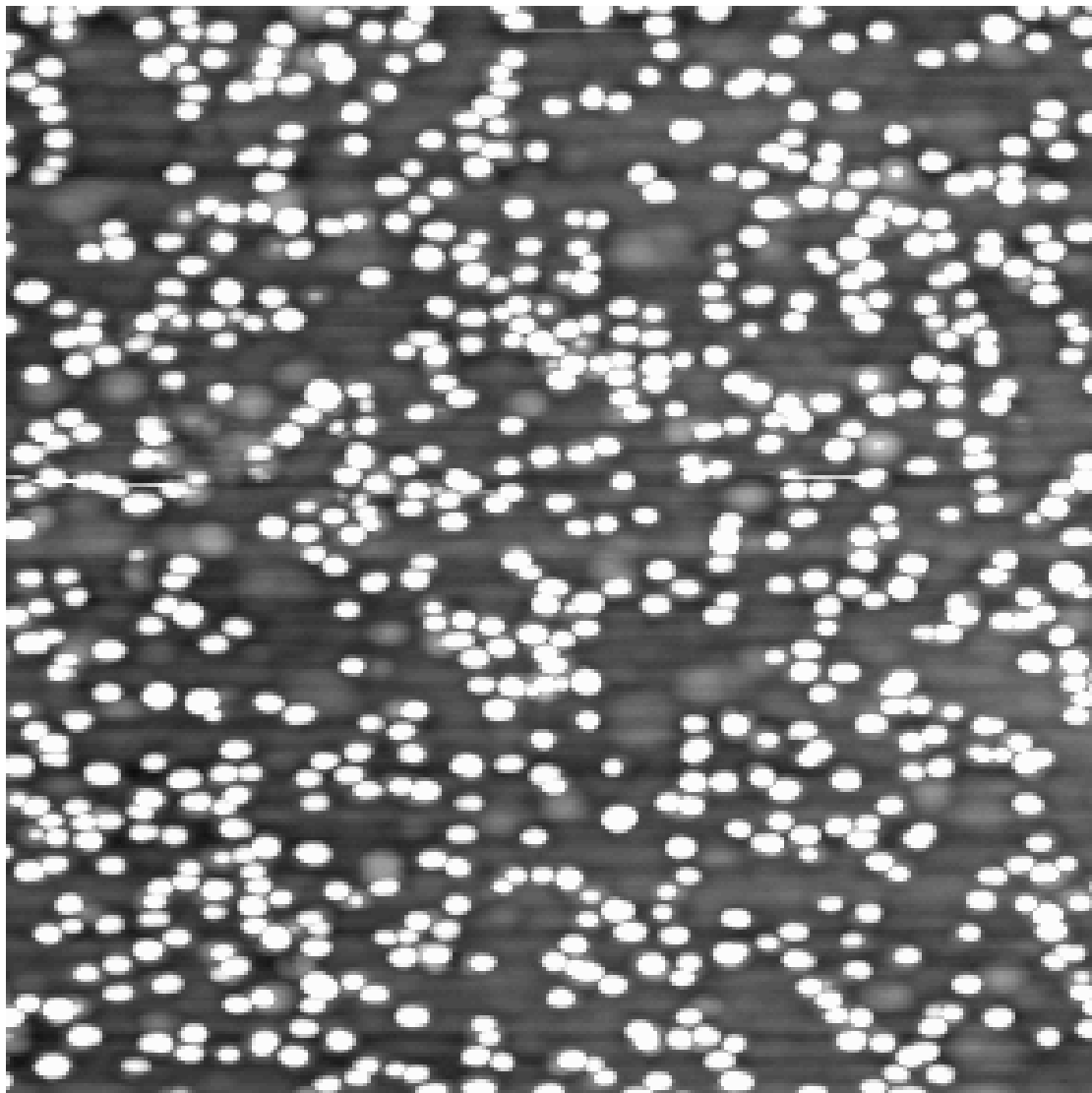


Figure 11 An AFM micrograph image of a region $2 \mu\text{m} \times 2 \mu\text{m}$ area of the QD structure resulting from the combined InAs SAQD and subsequent GaSb deposition. The inset is the RHEED image down the (110) direction of the sample showing elongated features at the 3D diffraction locations

surface morphology during growth of the GaSb crown as opposed to nucleation of additional features. The inset in Fig. 11, shows the RHEED pattern down the (110) direction of after the deposition of the 3ML of GaSb. It is observed that the typical chevron pattern has been replaced by large diffuse dashes at the 3D diffraction spots. The diffraction pattern down the perpendicular direction showed a similar broadening of the 3D spot. No square pyramidal structures indicative of the original InAs structure were observed after growth using AFM.

Coupled with the regularity of the QD shape (seen in Fig. 11) and the lack of InAs SAQD like structures remaining, these factors argue for the growth of the GaSb directly on the pre-existing InAs SAQDs. We propose this growth occurs due to preferential nucleation of the GaSb on the pre-existing InAs SAQDs. The InAs SAQDs act as nucleation sites due to the similar lattice constant between InAs and GaSb (6.0584Å and 6.095Å respectively). As has been observed and explained in the vertical stacking of QDs, the lowest energy position is the region, which has a lattice dimension closest to the material deposited⁵. In our case, the closest lattice match for the GaSb growth would be on the InAs SAQD. We view this to be a generic effect in the growth of the two similarly strained materials on a lower lattice constant substrate. Specifically we believe that nucleation of the second material is always possible on the original dot layer provided the strain and crystal structure are similar. Thus this procedure creates a method for constructing a quantum structure composed of different materials containing a heterojunction. We call this structure a Heterojunction Quantum Dot or HeQuAD.

Figure 12 is a (220) dark-field transmission electron microscope image showing the internal structure (cross-section) of a surface HEQUAD. It is evident that the HEQUAD consists of two distinct regions separated by well-defined facets of the type (001) on the top and low index facets on the sides. This is consistent with a HEQUAD structure that is composed of an InAs QD (inner) core and a GaSb (outer) crown. The contrast due to dislocations prominent in the core of the HEQUAD indicates significant relaxation of the InAs QD prior to deposition of the GaSb layer. It should be pointed out that, due to the arbitrariness in how the HEQUADs are sectioned during TEM sample preparation, the contrast in the core region of the HEQUAD is strongly influenced by the thickness of the surrounding GaSb crown.

To investigate the composition of the individual regions within the dot, X-ray energy dispersion spectrometry (XEDS) was performed using a nominal electron-beam probe size of 5 nm. The XEDS spectra were obtained by placing the probe at various locations corresponding to (a) the core region including the wetting layer of the HEQUAD, (b) (outer) periphery of the HEQUAD, and (c) in the GaAs cap away from the HEQUAD. The duration over which the spectra could be collected was however limited due to sample contamination

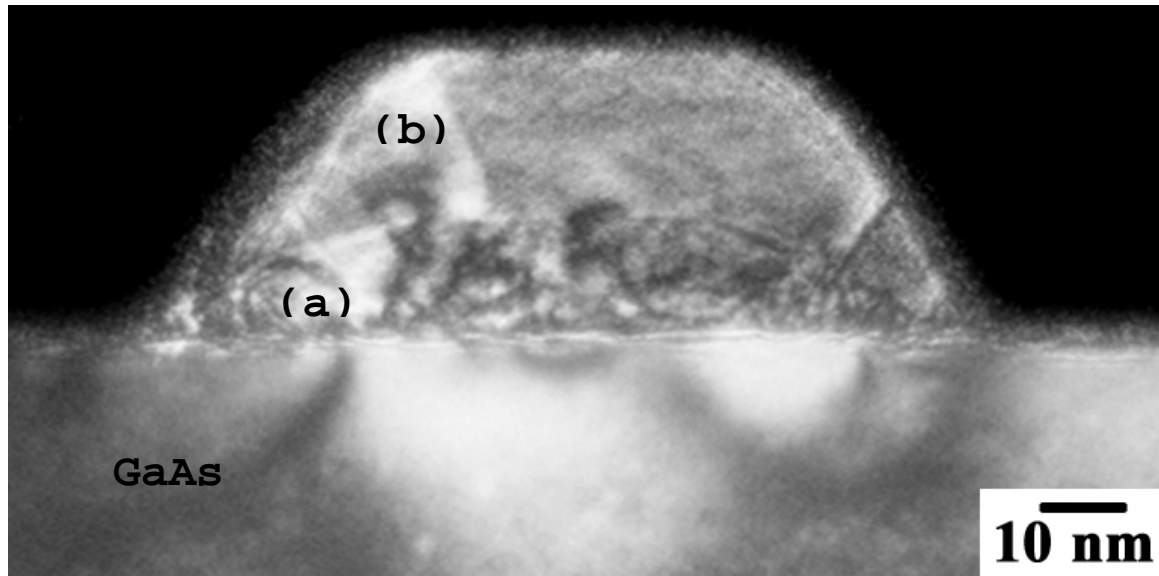


Figure 12. Cross sectional (220) dark-field transmission electron microscope micrograph showing the internal structure (cross-section) of a surface HEQUAD. The InAs core (a) is seen as a semi-spherical cap above the GaAs substrate and the GaSb crowns (b) the InAs

(specifically, Carbon build-up) and also sample degradation due to electron-beam irradiation. To enable a qualitative comparison of the spectra from different locations we examined differences in the intensities of the In- and Sb-K α peaks, using a reference spectrum obtained from the GaAs substrate. The results from the XEDS measurements are presented in Fig. 13. The results clearly reveal that the In-peak intensity is high in the core region of the HQUAD (“Dot + WL”). In contrast, the In-peak intensity at the periphery of the HQUAD is significantly reduced. On the other hand, intense Sb-peaks are observed in the periphery and in the core region of the HQUAD. However, we also observe that the Sb-peak within the core region has relatively stronger intensity than its corresponding In-peak. Hence, the intense Sb-peak from the core region of the HQUAD is attributed to the GaSb layer surrounding the InAs QD. These results further support our contention that the HQUAD is indeed composed of an InAs QD as its core and a GaSb layer as its shell.

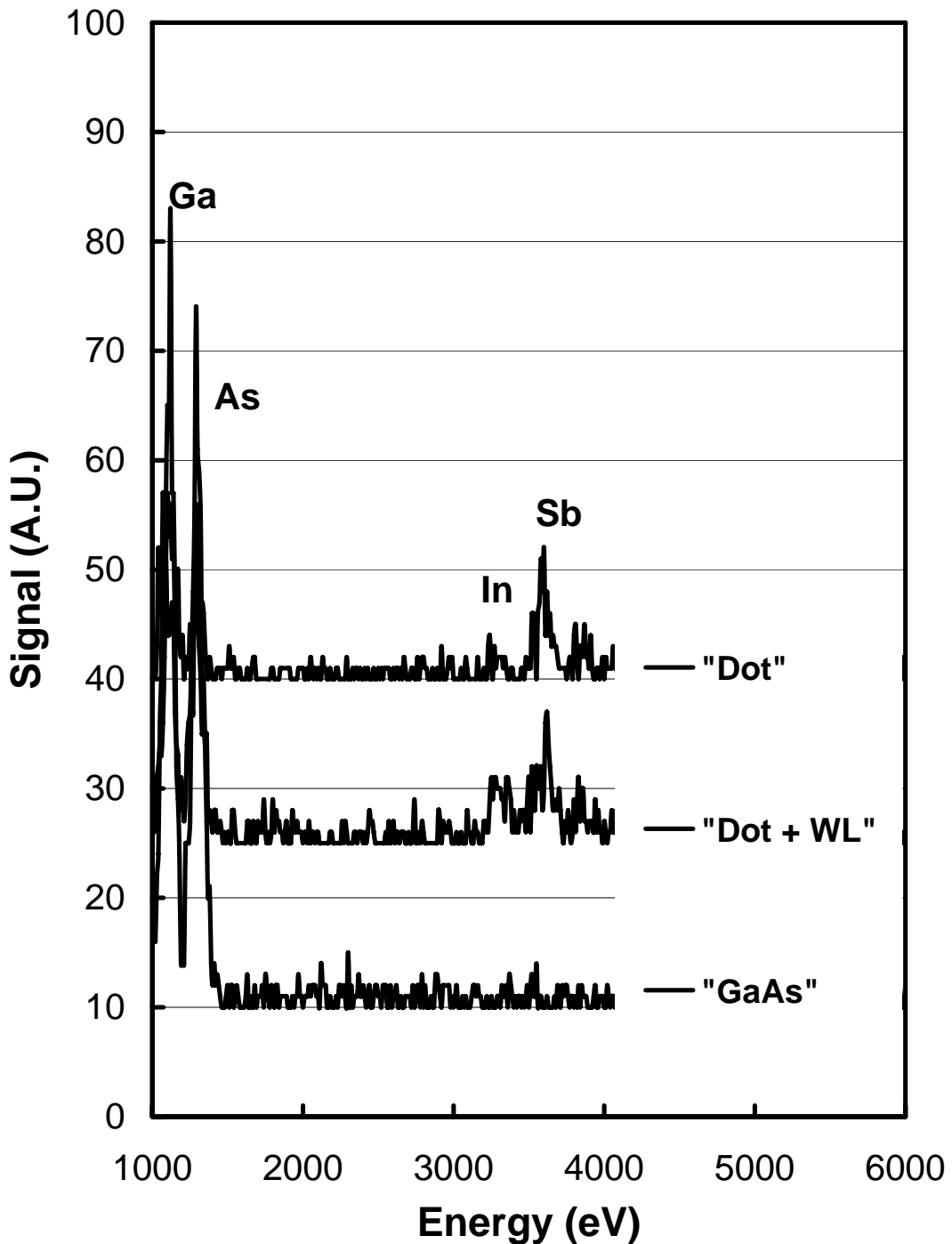


Figure 13 XEDS spectrum taken from various regions in the quantum dot structure.

CHAPTER 4

CONCLUSIONS

The major findings of the present study may be summarized as follows:

- We have demonstrated that EPWF retrieval from HRTEM images enables atomic resolution compositional mapping of quaternary III-V semiconductor interfaces with intermixing in both cation and anion sublattices. Using this approach we have independently quantified changes in the In-Ga and As-Sb contents across interfaces in an InAs/In_xGa_(1-x)Sb heterostructure, which revealed differences between the intermixing behavior within In-Ga and As-Sb sublattices of the individual interfaces.
- The studies on short period InAs/GaSb superlattices showed that the structural degradation, especially with respect to stability of interfaces, becomes significant as the period approaches 17Å. Improvement in the quality is realized when slower growth rates (for the GaSb layer) are employed.
- We have demonstrated the formation of a heterojunction quantum dot composed of a combination of GaSb and InAs. The composite GaSb/InAs dot is achieved by first forming an InAs QD via the conventional self-assembly process followed by the growth of a GaSb crown on the InAs QD structure. Transmission electron microscopy indicated a clear boundary between the GaSb and InAs regions with EDS showing an In rich core and an Sb rich cap.

REFERENCES

1. L. D. Nguyen, P. J. Tasker, and L. F. Eastman, IEEE Trans. Electron Devices **36**, 2243 (1989).
2. T. M. Cockermill, D. V. Forbes, J. A. Dantzig, and J. J. Coleman, IEEE J. Quantum Electron. **30**, 441 (1994).
3. F. Fuchs, u. Weimer, W. Pletschen, J. Schmitz, E. Ahlswede, M. Walther, J. Wagner, and P. Koidl, Appl. Phys. Lett. **71**, 3251 (1997).
4. G. W. Turner, H. K. Choi, and M. J. Manfra, Appl. Phys. Lett. **72**, 876 (1998).
5. X. Li, K. F. Longenbach, Y. Wang and W. I. Wang, IEEE Electron Device Lett. **13**, 192 (1992).
6. D. H. Chow, H. L. Dunlap, W. Williamson III, S. Enquist, B. K. Gilbert, S. Subramaniam, P. M. Lei, and G. H. Bernstein, IEEE Electron Device Lett. **17**, 69 (1996).
7. A. Ourmazd, D. W. Taylor, J. Cunningham and C. W. Tu, Phys. Rev. Lett. **62**, 933 (1989).
8. A. Ourmazd, F. H. Baumann, M. Bode, and Y. Kim, Ultramicroscopy **34**, 237 (1990).
9. S. Thoma and H. Cerva Ultramicroscopy **38**, 264 (1991).
10. A. Rosenauer, T. Remmele, D. Gerthsen, K. Tillman, and A. Forster, Optik **105**, 99 (1997).
11. A. Rosenauer and D. Gerthsen, Ultramicroscopy **76**, 49 (1999).
12. K. Mahalingam, "Stoichiometry of Interfaces in AlGaAs/GaAs Heterostructures grown by Molecular Beam Epitaxy," Air Force Research Laboratory Technical Report, Wright Patterson AFB, Task 99 (1998).
13. K. Mahalingam, "Transmission Electron Microscopy of III-V Heterostructures," Air Force Research Laboratory Technical Report, Wright Patterson AFB, Task 150 (1999).
14. D. B. Williams and C. B. Carter, "Transmission Electron Microscopy," Plenum Press, New York (1996).

15. A. Orchowski, W. D. Rau, H. Lichte, Phys. Rev. Lett. **74**, 399 (1995).
16. W. M. J. Coene, A. Thust, M. Op de Beeck, and D. Van Dyck , Ultramicroscopy **64**, 109 (1996).
17. A. Thust, W. M. J. Coene, M. Op de Beeck, D. Van Dyck, Ultramicroscopy **64**, 167 (1996).
18. C. L. Jia, R. Rosenfield, A. Thust and K. Urban, Phil. Mag. Lett. **79**, 99 (1999).
19. R. Rosenfield, A. Thust, W. Yang, M. Feuerbacher and K. Urban, Phil. Mag. Lett. **78**, 127 (1998).
20. C. L. Jia and A. Thust, *Phys. Rev. Lett.* **82**, 5052 (1999).
21. A. O'keefe, C. J. D. Hetherington, Y. C. Wang, E. C. Nelson, J. H. Turner, C. Kisielowski, J. O-Malm, R. Mueller, J. Ringnalda, M. Pan and A. Thust, Ultramicroscopy **89**, 215 (2001).
22. C. Kisielowski, C. J. D. Hetherington, Y. C. Wang, R. Kilaas, M. A. Okeefe and A. Thust, Ultramicroscopy **89**, 243 (2001).
23. M. A. Okeefe, *High-Resolution Transmission Electron Microscopy and Associated Techniques*, ed. P. Buseck, J. Cowley and L. Eyring (Oxford University Press, 1988) pp. 244.
24. *TrueImage* is a commercial software package distributed by FEI Inc, Portland, Oregon.
25. R. Kilaas, J. Microscopy **190** 45 (1998).
26. J. Steinshnider, J. Harper, M. Weimer, C. -H. Lin, and S. S. Pei, Phys. Rev. Lett. **85**, 4562 (2000) and references therein.
27. J. L. Rouviere and N. Bonnet, Inst. Phys. Conf. Ser. **134**, 11 (1993).
28. J. F. Aebersold, P. A. Stadelman, and J. L. Rouviere, Ultramicroscopy **62**, 171 (1996).
29. P. Trebbia and N. Bonnet, Ultramicroscopy **34**, 165 (1990).
30. K. Mahalingam, K. G. Eyink, G. J. Brown, and D. L. Dorsey, Int. J. Nanosci. **3**, 723 (2004).

31. The amorphous layers were simulated using the *MacTempas* software developed by Roar Kilaas, Total Resolution Inc., California.
32. O. G. Schmidt, Ch. Deneke, S. Kiravittaya, R. Songmuang, H. Heidemeyer, Y. Nakamura, R. Zapf-Gottwick, C. Müller, and N. Y. Jin-Phillipp , IEEE Journal of Selected Topics in Quantum Electronics **8**, 1025 (2002).
33. H. Mariette, C. R. Physique **6**,23–32 (2005).
34. J. Stangl, V. Holý, and G. Bauer, Rev. of Modern Physics, **76**, 725 (2004).
35. V. G. Dubrovskii, G. E. Cirlin, Yu. G. Musikhin, Yu. B. Samsonenko, A.A. Tonkikh, N. K. Polyakov, V. A. Egorov, A. F. Tsatsul'nikov, N. A.Krizhanovskaya, V. M. Ustinov, and P. Werner, J. Cryst. Growth 267, 2004
36. Q. Xie, A. Madhukar, P. Chen, and N. Kobayashi, Phys. Rev. Lett. **75**, 2542 (1995).
37. L. Müller-Kirsch, N.N. Ledentsov, R. Sellin, U.W. Pohl, D. Bimberg, I. Hausler, H. Kirmse, and W. Neumann, J. Cryst. Growth **248**, 333 (2003).
38. Y. Liu, M. Hopkinson, C. N. Harrison, M. J. Steer, R. Frith, I. R. Sellers, D. J. Mowbray, and M. S. Skolnick, J. Appl. Phys. **93**, 2931 (2003).
39. Ledentsov, D. Bimberg, V. M. Ustinov, Zh. I. Alferov, and J. A. Lott, Physica E **13**, 871 (2002).
40. J. W. Lee, D. Schuh, M. Bichler, and G. Abstreiter, Appl. Surf. Sci. **228**, 306 (2004).
41. D. W. Pashley, J. H. Neave, and B. A. Joyce, Surf. Sci. **476**, 35(2001).